Cellular correlate of assembly formation in oscillating hippocampal networks in vitro

Florian Bähner[a], Elisa K. Weiss[a], Gunnar Birke[a], Nikolaus Maier[b], Dietmar Schmitz[b], Uwe Rudolph[c], Michael Frotscher[d,e], Roger D. Traub[f], Martin Both[a,1], and Andreas Draguhn[a,1,2]

[a]Institute of Physiology and Pathophysiology, Medical Faculty, University of Heidelberg, D-69120 Heidelberg, Germany; [b]Neurowissenschaftliches Forschungszentrum, Charité-Universitätsmedizin Berlin, Cluster of Excellence, NeuroCure, D-10117 Berlin, Germany; [c]Laboratory of Genetic Neuropharmacology, McLean Hospital, Department of Psychiatry, Harvard Medical School, Belmont, MA 02478; [d]Institute of Anatomy and Cell Biology, University of Freiburg, D-79104 Freiburg, Germany; [e]Center for Molecular Neurobiology Hamburg, D-20251 Hamburg, Germany; and [f]IBM T. J. Watson Research Center, Yorktown Heights, NY 10598

Edited by* N. Kopell, Boston University, Boston, MA, and approved June 20, 2011 (received for review March 4, 2011)

Neurons form transiently stable assemblies that may underlie cognitive functions, including memory formation. In most brain regions, coherent activity is organized by network oscillations that involve sparse firing within a well-defined minority of cells. Despite extensive work on the underlying cellular mechanisms, a fundamental question remains unsolved: how are participating neurons distinguished from the majority of nonparticipators? We used physiological and modeling techniques to analyze neuronal activity in mouse hippocampal slices during spontaneously occurring high-frequency network oscillations. Network-entrained action potentials were exclusively observed in a defined subset of pyramidal cells, yielding a strict distinction between participating and nonparticipating neurons. These spikes had unique properties, because they were generated in the axon without prior depolarization of the soma. $GABA_A$ receptors had a dual role in pyramidal cell recruitment. First, the sparse occurrence of entrained spikes was accomplished by intense perisomatic inhibition. Second, antidromic spike generation was facilitated by tonic effects of GABA in remote axonal compartments. Ectopic spike generation together with strong somatodendritic inhibition may provide a cellular mechanism for the definition of oscillating assemblies.

antidromic action potentials | CA1 pyramidal cells | interneurons | ripples

Information processing in neuronal networks has been proposed to rely on coordinated patterns of activity in transiently stable neuronal assemblies (1). Such patterns underlie different cognitive or behavioral tasks including motor patterns (2), perception (3), and spatial cognition (4). The functional coupling of neurons within distributed assemblies is believed to be organized by network oscillations that cover multiple frequency bands and follow distinct mechanisms (5). However, it is still unclear how neurons within an activated assembly are distinguished from the majority of nonparticipating cells. This distinction is essential for maintaining sparse and stable neural representations (6).

Spatial memory formation in rodents has become an important model system for studying neuronal representations within networks. Place-selective neurons of the hippocampus are sequentially activated during exploration of an environment and reactivated during subsequent resting periods (7), indicating the formation of stable assemblies. During reactivation, temporal and spatial precision of pyramidal cell firing is organized by propagating sharp waves with superimposed high-frequency network oscillations [sharp wave ripple complexes (SPW-Rs)] (8, 9). While traveling through the CA1 area, each SPW-R recruits only a few selected cells to fire action potentials (8), whereas the majority of nonparticipating cells is silent, ensuring clear signal to noise separation (10). The mechanisms underlying this functional distinction between participating and nonparticipating cells are, however, unclear. Recordings in vivo (11) and in vitro (12) have provided strong evidence for a major role of inhibitory interneurons in the temporal organization of cortical oscillations. In addition, electrical coupling between axons has been suggested to mediate the coordination of pyramidal cell activity during fast network oscillations (13), consistent with recent reports of nonconanical mechanisms of action potential generation in CA1 pyramidal cells in vivo (14) and in vitro (15, 16). We used an in vitro model of SPW-Rs to unravel the mechanisms underlying selection of participating CA1 pyramidal cells. Action potentials of SPW-R–entrained neurons were generated ectopically in distal axonal compartments. Activation of axonal $GABA_A$ receptors facilitated spiking, whereas strong concomitant perisomatic inhibition efficiently suppressed background activity.

Results

CA1 Pyramidal Cells Form Two Functionally Distinct Subgroups During SPW-Rs. Spontaneously occurring field events in mouse hippocampal brain slices resemble characteristic properties of SPW-Rs in vivo (10). We recorded such field potentials in the CA1 pyramidal cell layer together with intracellular potentials of 153 CA1 pyramidal neurons (*Materials and Methods* and *SI Materials and Methods*). At resting membrane potential, network-correlated action potentials were observed in 41% of the cells. Each participating cell fired only on a minority of SPW-Rs (Figs. 1*A* and 2 *A* and *B*). Median discharge probability was one action potential on 1.6% of sharp waves (median; P_{25} = 0.3% and P_{75} = 6%), corresponding to a firing rate of 0.038 Hz (median; P_{25} = 0.01 Hz and P_{75} = 0.15 Hz). This value is more than fivefold higher than the firing rate outside sharp wave episodes (0.007, 0.001, and 0.022 Hz) (Fig. 2*B*). SPW-R–associated action potentials were strongly phase-coupled to the ∼200-Hz network ripples (Fig. 1 *A*, *C*, and *E*). During single ripple cycles, 50% of action potentials occurred within 1.06 ms (0.98–1.26 ms), corresponding to 26.4 ± 2.4% of a ripple cycle (n = 13 cells). This temporal precision (9) is in marked contrast to the reported large temporal jitter of excitatory postsynaptic potential (EPSP)-evoked spikes in CA1 pyramidal cells (17).

Passive membrane properties were not different between participating and nonparticipating cells (Fig. S1). Interestingly, nonparticipating cells could not be recruited into SPW-Rs by somatic depolarization (Fig. 2*C*). Although injection of positive current enhanced basal firing rates of both participating and

Author contributions: F.B., D.S., R.D.T., and A.D. designed research; F.B., E.K.W., G.B., N.M., M.F., R.D.T., and M.B. performed research; U.R. contributed new reagents/analytic tools; F.B., E.K.W., G.B., N.M., D.S., M.F., R.D.T., and M.B. analyzed data; and F.B., R.D.T., M.B., and A.D. wrote the paper.

The authors declare no conflict of interest.

*This Direct Submission article had a prearranged editor.

[1]M.B. and A.D. contributed equally to this work.

[2]To whom correspondence should be addressed. E-mail: andreas.draguhn@physiologie.uni-heidelberg.de.

This article contains supporting information online at www.pnas.org/lookup/suppl/doi:10.1073/pnas.1103546108/-/DCSupplemental.

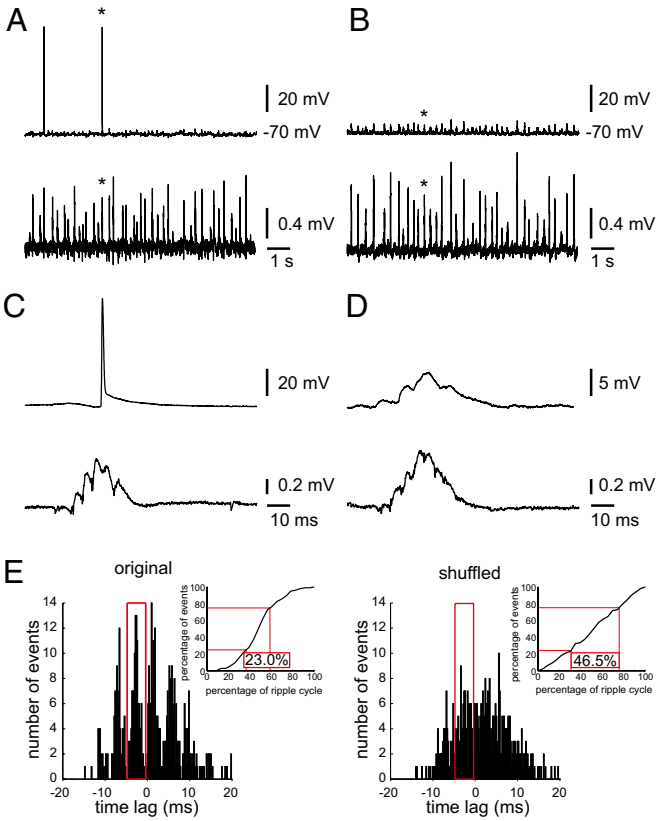

Fig. 1. Firing patterns of CA1 pyramidal cells during SPW-Rs. (*A*) Original recordings from a cell that participates in SPW-Rs. *Upper* shows intracellular recording with two action potentials, and *Lower* shows field sharp wave ripple complexes. (*B*) Original recording from a cell (*Upper*) that does not fire during SPW-Rs (*Lower*). (*C*) Expanded trace from the cell in *A* showing an action potential during the field SPW-R (marked with an asterisk in *A*). (*D*) Expanded trace from the nonparticipating cell shown in *B*. The sharp wave is accompanied by a subthreshold synaptic potential. (*E Left*) Event cross-correlogram showing precision of firing during SPW-Rs (data from the cell shown in *A* and *C*). (*Left Inset*) Cumulative plot of spikes within one ripple cycle (red box around the central peak of the cross-correlogram). In this cell, 50% of action potentials occurred within 23% of a full ripple cycle, indicating strong phase-coupling to ripples. (*Right*) Loss of phase coupling on shuffling of spikes and ripples. Cross-correlogram was constructed between spikes and ripples from the subsequent SPW-R event. Cumulative plot (*Right Inset*) shows loss of coupling.

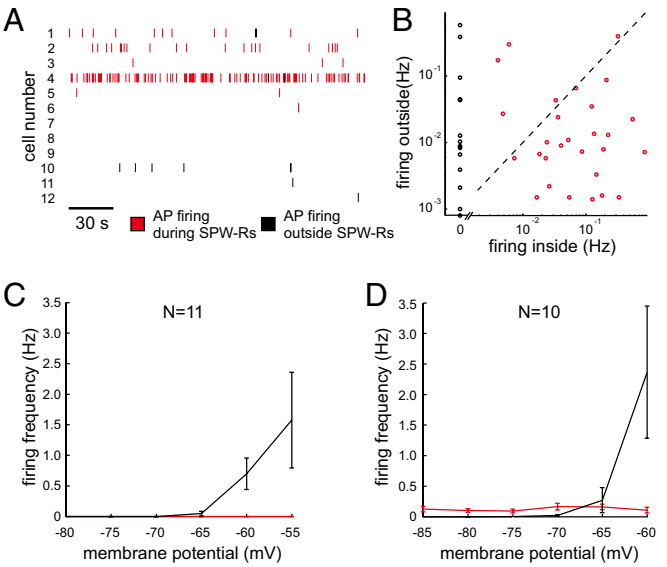

Fig. 2. CA1 pyramidal cells form two functionally distinct subgroups during SPW-Rs. (*A*) Raster plot of action potentials from participating cells (1–6) and nonparticipating cells (7–12). Red ticks indicate phase-coupled action potentials during ripples, and black ticks are noncoupled action potentials. (*B*) Basal firing rates are plotted over firing rates during SPW-Rs for both participating (red circles) and nonparticipating (black circles) neurons. Note that most participating cells fire at a much higher rate during ripples (red circles on the right side of the dotted line). (*C*) Firing rate of nonparticipating cells at different membrane potentials. Depolarization increases firing (black curve) but does not induce any SPW-R–coupled spikes (red curve), indicating high signal to noise separation during SPW-Rs. (*D*) Firing rate of participating cells at different membrane potentials. Although basal action potential frequency increases on depolarization, spiking during ripples is largely independent of somatic membrane potential.

nonparticipating cells, SPW-R–coupled spikes were independent of membrane potential (Fig. 2*D* and Fig. S2*A*). Together, these data show that CA1 pyramidal cells form two clearly distinct functional groups with respect to their participation in SPW-Rs.

SPW-R–Coupled Action Potentials Are Antidromic Spikes. Action potentials outside and inside SPW-Rs had strikingly different waveforms. Ripple-associated spikes arose abruptly from a presumably $GABA_A$ receptor-mediated fast hyperpolarization (reversal potential = -72.3 ± 1.0 mV; $R = -0.83 \pm 0.04$; $n = 5$ cells) (Fig. 3 *A* and *B* and Fig. S2*B*). They were followed by a depolarizing afterpotential that decayed with $\tau = 4.9 \pm 0.3$ ms ($n = 16$ cells). In contrast, noncoupled action potentials emanated from a slow depolarization and were followed by a fast and medium afterhyperpolarization (Fig. 3 *A* and *B*) (18). Firing threshold of SPW-R–coupled spikes was -66.4 ± 1.2 mV ($n = 17$ cells), which is about 19 mV more negative than the threshold for action potentials occurring outside ripples (-47.8 ± 1.4 mV, $n = 14$ cells; $P = 5.6 \times 10^{-11}$, unpaired *t* test) (details on spike properties in Fig. S3). Together, this waveform is strongly reminiscent of antidromically generated action potentials (16, 19–21).

Action potentials are usually generated in the initial segment (IS spike) before back-propagating into the somatodendritic compartment (SD component) (22). The depolarizing postsynaptic potentials preceding spike generation precharge the somatodendritic capacitor before reaching the initial segment. This precharging is missing in antidromic action potentials, thus enhancing the latency between spike generation (IS spike) and the somatodendritic component (SD). IS-SD latency can, therefore, be used as a marker for antidromic spikes (20, 22). Indeed, the second derivative of SPW-R–coupled action potentials showed two components with a clear phase lag that was largely absent in spikes outside SPW-Rs (Fig. 3*C*). The antidromic nature of SPW-R–coupled spikes was also reflected by the appearance of a notch on the ascending phase in 4 of 17 neurons measured at hyperpolarized potentials, again indicative of IS-SD breaks (Fig. S4) (19–21). SPW-R–related spikes persisted even on strong hyperpolarization by up to −30 mV (Fig. 2*D* and Fig. S2*A*), but they were sometimes replaced by phase-coupled partial spikes (3 of 17 cells) (Fig. S4*A*). For direct comparison, we evoked orthodromic and antidromic spikes by electrical stimulation in stratum radiatum or the alveus, respectively. As expected, Schaffer collateral-evoked orthodromic action potentials matched properties of spontaneous spikes outside SPW-Rs, whereas antidromically evoked spikes showed the characteristic features of ripple-entrained action potentials (Fig. S5). Interestingly, antidromic spikes could be evoked during and outside spontaneous network events ($n = 6$) (Fig. S5). In contrast, orthodromic spikes could not be elicited by somatic current injection during SPW-Rs (Fig. 2*C* and Fig. S5*F*).

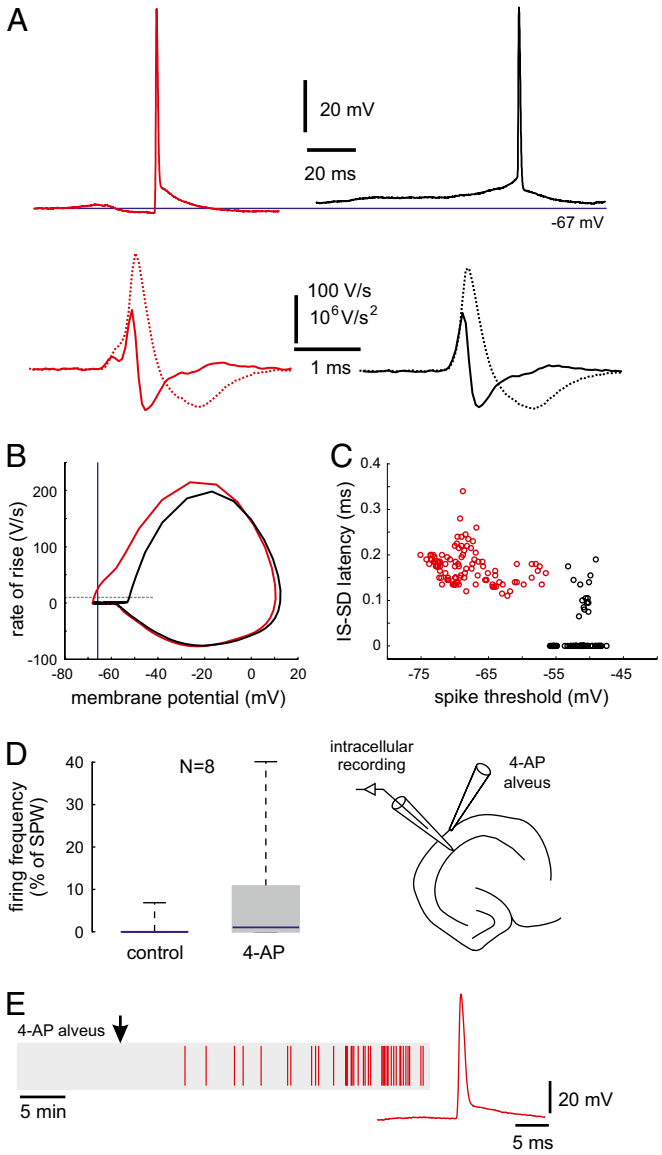

Fig. 3. SPW-R–coupled action potentials are antidromic spikes. (*A Upper*) Action potentials within (*Left*) and outside (*Right*) SPW-Rs taken from a single participating neuron. The blue line indicates resting membrane potential. Note the hyperpolarizing prepotential, sharp onset, and depolarizing afterpotential of the SPW-R–coupled spike. (*Lower*) First (dotted line) and second (solid line) temporal derivative of the action potential within (*Left*) and outside (*Right*) ripples. Note the prominent separation of the IS and SD component of the ripple-associated spike, which is a typical feature of antidromic spikes. (*B*) Phase plot (dV/dt vs. V) of action potentials shown in *A*. The blue line represents resting membrane potential. The dotted line indicates threshold, defined as dV/dt = 10 V/s. Note the negative shift of threshold for the SPW-R–coupled action potential. (*C*) IS-SD latency is plotted over spike threshold for individual action potentials during or outside ripples, respectively (10 cells for each group). Action potentials during and outside SPW-Rs clearly fall into two nonoverlapping clusters. (*D Left*) Increased firing frequency during ripples on application of 4-AP into the alveus. (*Right*) Experimental setup showing the intracellular recording pipette in stratum pyramidale and the application pipette in the alveus. (*E*) Raster plot of action potentials from a nonparticipating cell that started to fire phase-locked antidromic spikes after application of the drug.

Antidromic spikes can be elicited by blocking axonal potassium channels (23). Local application of 4-aminopyridine (4-AP; 100 μM) into the alveus increased firing frequency during SPW-Rs in five of eight cells (control: median = 0.0% of SPW-Rs with spikes, P_{25} = 0.0%, and P_{75} = 0.0%; 4-AP: median = 1.0%, P_{25} = 0.0%, and P_{75} = 10.8%) (Fig. 3 *D* and *E*). More than 98% of the induced antidromic spikes were entrained by the network rhythm. Together, these data suggest that SPW-R–coupled action potentials are generated in the axon without prior somatic depolarization. Antidromic action potentials are a distinguishing feature of CA1 pyramidal cells that participate in SPW-Rs.

Discharge Probability of All Pyramidal Cells Is Controlled by Strong Perisomatic Inhibition During Ripples. Juxtacellular recordings from putative interneurons revealed high-frequency firing at earlier phases of sharp waves than pyramidal neurons (n = 19 cells) (Fig. 4), similar to findings in vivo (9, 11). In contrast to pyramidal cells, interneurons were activated on the majority of SPW-Rs (83.6 ± 3.9%) and typically emitted multiple spikes (1.9 ± 0.2 spikes per SPW-R). Spikes were strongly coupled to individual ripple cycles (coupling strength = 25.1 ± 2.0%; not different from participating pyramidal cells, P = 0.67, unpaired t test). Light microscopy of juxtacellularly labeled cells revealed somata within or close to the pyramidal cell layer, radially oriented dendritic trees, and axonal ramifications in the somatic and proximal dendritic layers, indicative of perisomatically inhibiting interneurons. Four cells with axonal projection patterns in basal portions of the pyramidal cell layer were analyzed at the ultrastructural level. All examined postsynaptic contacts were confined to the perisomatic region or proximal dendrites (Fig. 4*A*), and the cells were, therefore, classified as basket cells. These data are in line with recent findings from in vivo recordings indicating that perisomatically inhibiting neurons are highly active during SPW-Rs, whereas axoaxonic cells do not participate (11). In addition, we performed whole-cell recordings from eight fast-spiking interneurons (Fig. 4 *D–F*) (24). Recordings in both current and voltage clamp indicated that these cells receive excitatory inputs at ripple frequency, which causes multiple orthodromic spikes during each network event (Fig. 4 *E* and *F*).

The strong perisomatic inhibition during SPW-Rs was reflected by a conductance increase of participating and nonparticipating pyramidal cells (153 ± 7.6% and 156.3 ± 6.6% of baseline conductance, respectively; n = 9 cells each; P = 0.75, unpaired t test) (Fig. 5*A*). Reversal potential of subthreshold SPW-R–coupled potentials was −70.2 mV (−73.6 to −64.8 mV; n = 9) in participating and −68.4 mV (−69.1 to −65.5 mV) in nonparticipating cells (n = 9; P = 0.26, Mann–Whitney u test) (Fig. 5*A*). Thus, participating and nonparticipating cells receive comparably strong somatodendritic GABAergic input during SPW-Rs, consistent with data from in vivo recordings (8, 11). The inhibitory role of GABAergic hyperpolarization became apparent in recordings with chloride-filled electrodes that shifted the GABAergic reversal potential to more positive values (n = 14 cells) (Fig. 5*B*). Under these conditions, all pyramidal cells fired at high frequency during most of the SPW-R events (66.8 ± 8.2% of SPW-Rs, firing frequency during SPW-Rs = 4.920 ± 0.918 Hz). Tight coupling of neurons to the network rhythm was maintained [50% of action potentials within 1.21 ms (1.12–1.28 ms) of a ripple cycle; coupling strength = 25 ± 2.3%].

This notion was confirmed by recordings with intracellular application of the $GABA_A$ receptor blocker picrotoxin (200 μM) (25). Basal activity outside SPW-Rs was not affected by the drug, whereas 11 of 24 cells showed a continuous increase in ripple-coupled action potentials during diffusion of the drug into somatodendritic compartments (control: median = 0.0% of SPW-Rs with spikes, P_{25} = 0.0%, and P_{75} = 0.0%; picrotoxin: median = 0.0%, P_{25} = 0.0%, and P_{75} = 0.6%; $P = 10^{-3}$, Wilcoxon matched-pairs signed-ranks test) (Fig. 5 *C* and *D*). Cells that were recorded without the addition of picrotoxin did not show such a time-dependent increase in SPW-R–associated firing (n = 7). Thus, efficient perisomatic inhibition is crucial

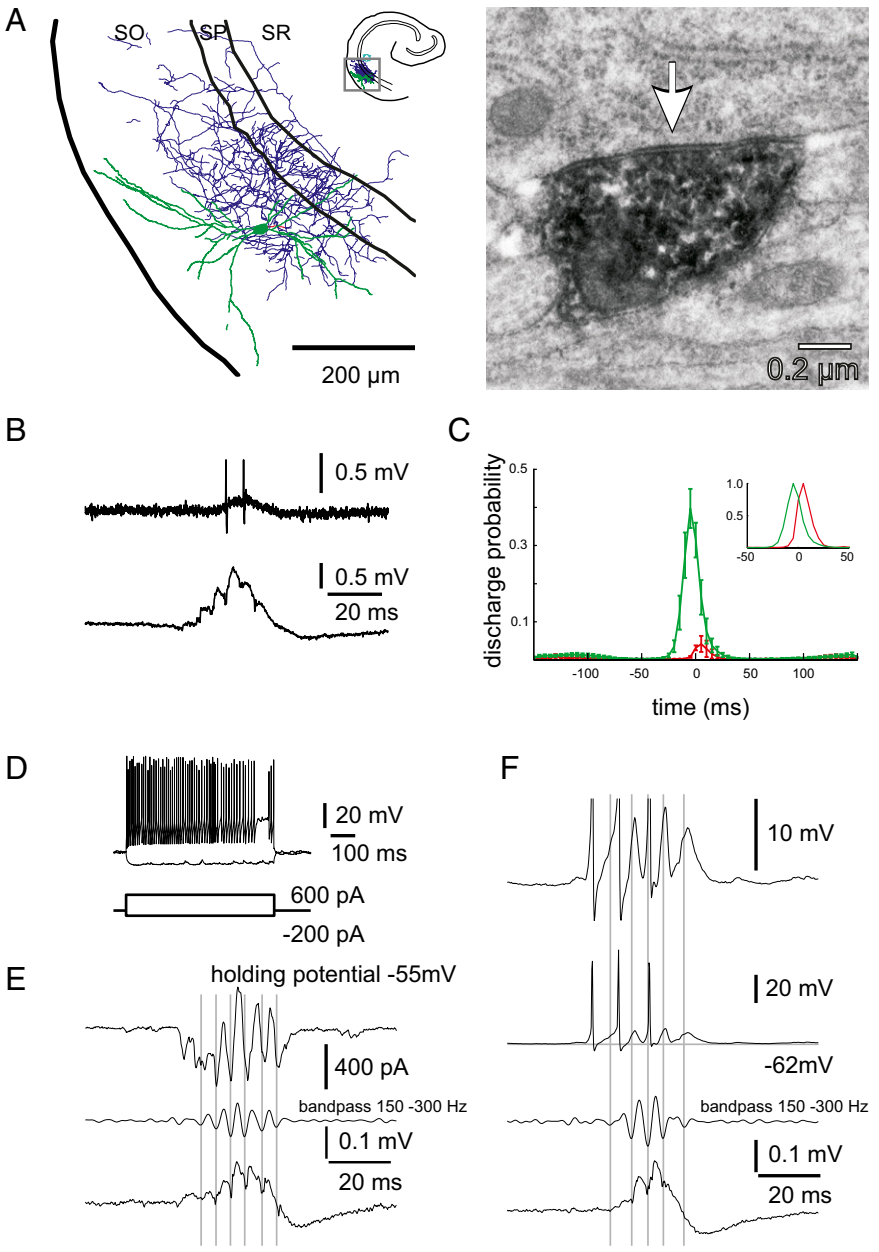

Fig. 4. Phase-locked high-frequency firing of perisomatic-targeting interneurons during ripples. (*A Left*) Reconstruction of a biocytin-labeled basket cell in CA1 (only one section of 70 µm thickness is shown). Soma and dendrites are in green, and axons are in blue. (*Right*) Axosomatic synapse formed by the biocytin-labeled basket cell terminal and a postsynaptic pyramidal cell. The arrow indicates symmetric synaptic contact; 14 synaptic contacts were evaluated at the ultrastructural level and determined to be either axodendritic (n = 8) or axosomatic (n = 6). (*B*) Juxtacellular recording from the basket cell shown in *A*, which emits two spikes (*Upper*) during an SPW-R (*Lower*). This cell fired during 81.7% of SPW-Rs and was tightly coupled to the network rhythm (coupling strength was 23.4%). (*C*) Event cross-correlation between action potentials and the peak of SPW-Rs from pyramidal cells (n = 13; red) or interneurons (n = 19; green). Both cell types have their highest firing probability around the peak of the sharp wave. (*Inset*) The same data with peaks normalized to one. Note that interneurons fire earlier than pyramidal cells. (*D*) Whole-cell recording from a fast-spiking interneuron. (*E*) Voltage clamp. At a holding potential of −55 mV, rhythmically alternating inward and outward currents (*Top*) can be recorded during an SPW-R event (*Bottom*), indicating both excitatory and inhibitory input at network frequency. (*Middle*) Band pass-filtered field potential. Verticals are aligned with the ripple trough. (*F*) Current clamp. Original trace from the same cell showing three action potentials and accompanying synaptic potentials (top traces) during an SPW-R (bottom trace). Note that large excitatory postsynaptic potentials occur at ripple frequency and precede each phase-locked orthodromic spike.

for maintaining a sparse firing mode of selected pyramidal cells during SPW-Rs (see also Fig. S6).

Tonic Activation of Axonal $GABA_A$ Receptors Is Necessary for the Generation of Antidromic Action Potentials During SPW-Rs. High-frequency discharges of inhibitory interneurons in CA1 elevate ambient GABA concentrations and cause tonic activation of $GABA_A$ receptors (26). In stratum oriens, this mechanism induces high-frequency network activity by increasing axonal excitability (27), whereas basal dendrites in the same layer are hyperpolarized by activation of $GABA_A$ receptors (28). In the absence of classical somatic EPSP spike sequences, we reasoned that similar mechanisms could contribute to antidromic spike generation during SPW-Rs. We, therefore, locally applied muscimol (5 µM) to stratum oriens. Indeed, this agent induced phase-coupled action potentials in six of seven nonparticipating

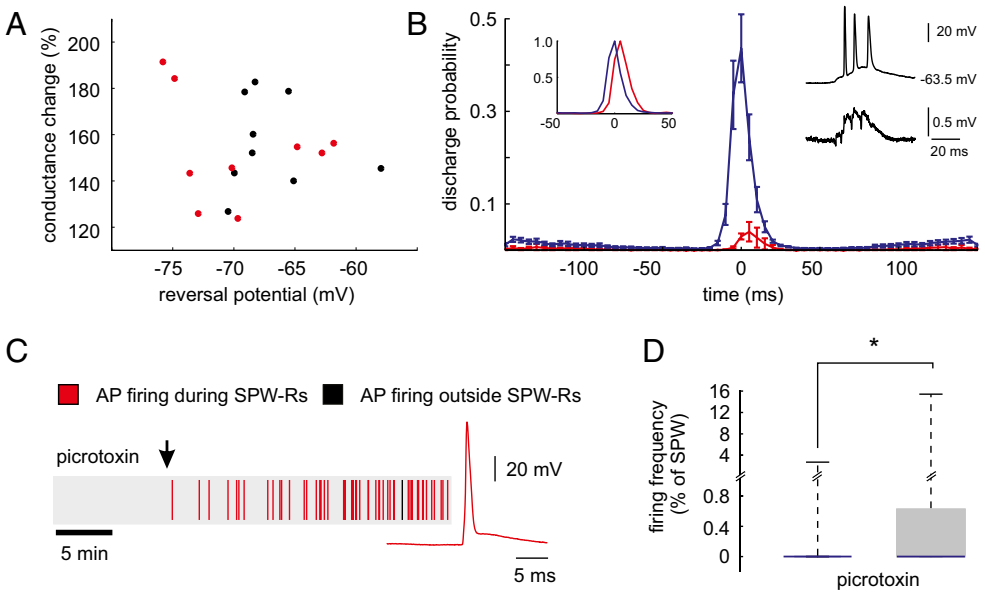

Fig. 5. Discharge probability of pyramidal cells is controlled by strong synaptic inhibition during ripples. (*A*) Synaptic input of participating (n = 9; red circles) and nonparticipating (n = 9; black circles) cells at the peak of SPW-Rs. Both reversal potential and conductance change (i.e., amount of synaptic input) are not different between groups. Note that, in most neurons, the reversal potential during SPW-Rs is close to the reversal potential of the $GABA_A$ receptor. (*B*) Event cross-correlation between the peak of the SPW-R and action potentials from pyramidal cells recorded with KAc-filled (n = 13; red) or KCl-filled (n = 14; blue) electrodes (on the left). Although all pyramidal cells have their highest firing probability around the peak of SPW-Rs, the discharge probability for cells with a depolarized GABAergic reversal potential is massively increased. (*Inset Left*) Both peaks were normalized to one. Note that discharge of pyramidal cells recorded with KCl-filled electrodes peaks earlier. (*Inset Right*) Original trace of a pyramidal cell recorded with a KCl-filled electrode (*Inset Right Upper*) and corresponding field potential (*Inset Right Lower*). The cell fired on 98.3% of SPW-R and emitted 2.7 spikes per SPW-R, underlining the critical role of perisomatic inhibition for signal to noise ratio. (*C*) Raster plot of action potentials from a cell recorded with a KAc-filled electrode. Picrotoxin (200 μM) was added to the pipette solution. Note the recruitment of the nonparticipating cell ~10 min after impalement. *Right* shows a typical coupled action potential from the cell. (*D*) Ripple-associated firing increases after impalement.

cells and increased SPW-R–related firing rates in three of three participating cells (Fig. 6 *A* and *B*). As a group, spike occurrence during SPW-Rs increased from 0% (median; 0.0–0.1%) to 0.4% (0.1–0.7%; n = 10; $P = 4 \times 10^{-3}$, Wilcoxon matched-pairs signed-ranks test). Similar to 4-AP, muscimol did not induce a significant increase in firing outside SPW-Rs.

α2-Subunit–containing $GABA_A$ receptors have been reported to be enriched in pyramidal cell axons (29–31). We made use of $GABA_AR\ \alpha2^{H101R}$ mice in which this receptor isoform is selectively insensitive to benzodiazepines (32). In WT mice, bath application of diazepam (20 μM) increased SPW-R–associated firing in three of three participating neurons, whereas firing outside SPW-Rs remained unchanged (Fig. 6*C* and Fig. S7). In addition, diazepam recruited three of five nonparticipating cells into SPW-Rs. Together, spike occurrence during SPW-Rs increased from a median value of 0% (0.0–0.9%) to 9% (0.9–10.6%; n = 8; P = 0.03, Wilcoxon matched-pairs signed-ranks test) (Fig. 6*C*). At the network level, diazepam did not change properties of individual SPW-R events (Fig. S7), whereas it decreased the frequency of occurrence of SPW-Rs, which was expected from a general reduction in excitability (from 1.60 ± 0.28 Hz to 1.23 ± 0.24 Hz; n = 8; $P < 0.05$). In slices from $\alpha2^{H101R}$ mice, sharp wave-associated spikes had the same antidromic waveform as observed in control tissue. Again, diazepam reduced the occurrence of SPW-Rs. In contrast with WT mice, CA1 pyramidal cells from slices of $\alpha2^{H101R}$ mice could not be recruited into SPW-Rs by application of diazepam (n = 5 nonparticipating cells). In all seven cells tested, SPW-R–coupled firing was not increased by diazepam, supporting the facilitating role of axonal $GABA_A$ receptors in spike generation (Fig. 6*D*) (median increase in $\alpha2^{H101R}$ mice = 0.0%, P_{25} = 0.0%, and P_{75} = 0.2%; P = 0.95, Mann–Whitney u test; different from increase in WT mice; P = 0.04, Mann–Whitney u test).

Finally, the differential GABAergic effects at axonal vs. proximal somatodendritic sites were validated by local application of GABAergic modulators (Fig. 7). Spatial restriction of drug applications was verified in experiments where we locally applied the fluorescent dye fluorescein (1 mM) (*SI Materials and Methods* and Fig. S8). Infusion of diazepam into stratum oriens increased ripple-associated firing in participating cells and induced SPW-R–associated action potentials in previously nonparticipating neurons (control: median = 0.1% of SPW-R with spikes, P_{25} = 0.0%;, and P_{75} = 0.4%; diazepam: median = 0.8%, P_{25} = 0.1%, and P_{75} = 2.3%; data from eight participators and seven nonparticipators; P = 0.03, Mann–Whitney test) (Fig. 7 *A* and *B*). In contrast, application of diazepam into stratum radiatum did not exert an effect on firing during ripples (control: median = 0.00%, P_{25} = 0.0%, and P_{75} = 0.1%; diazepam: median = 0.2%, P_{25} = 0.0%, and P_{75} = 0.6%; n = 4 participators and 7 nonparticipators; P = 0.22, Mann–Whitney test) (Fig. 7*A*). Conversely, suppression of GABAergic transmission by local application of gabazine into stratum oriens completely abolished ripple-associated spiking in participators (n = 4) (Fig. 7 *A* and *B*) in a reversible fashion. Local application of gabazine into stratum radiatum did not reduce but rather, increased the ripple-associated firing of participating cells (n = 4) (Fig. 7*A*).

These data indicate that axonal, α2-subunit–containing $GABA_A$ receptors potentiate the generation of SPW-R–coupled ectopic action potentials in both participating and previously nonparticipating neurons. In contrast, perisomatic GABAergic inhibition reduces firing probability of all pyramidal cells during SPW-Rs.

Simulation Results. Strong, rhythmic inhibition of pyramidal cells has been consistently observed in our experiments and in vivo (9, 11), and it has been proposed as the main mechanism for the

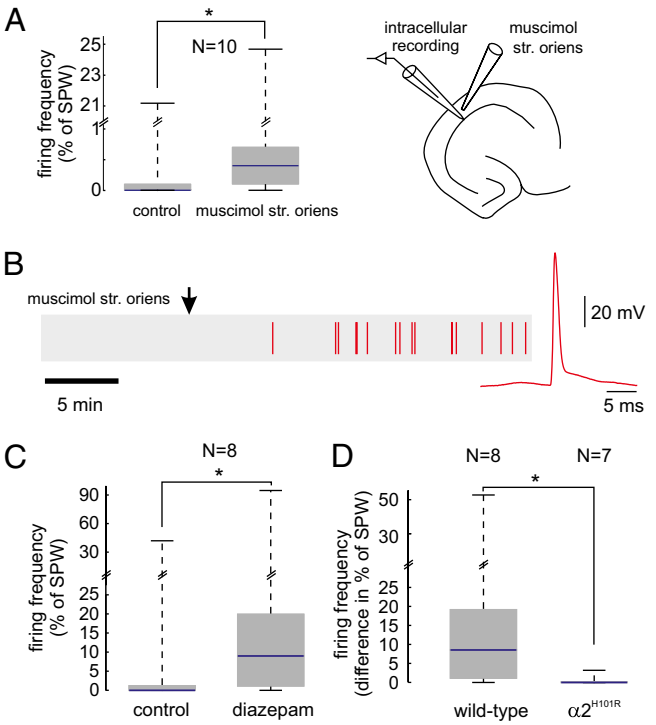

Fig. 6. Pyramidal cell recruitment is modulated by a subunit-specific tonic GABAergic input to the axonal compartment. (*A Left*) Application of muscimol into stratum oriens increases SPW-R–coupled firing in 9 of 10 cells (7 nonparticipating cells and 3 participating cells). (*Right*) Experimental setup showing the intracellular recording pipette in stratum pyramidale and the application pipette in stratum oriens, respectively. (*B*) Raster plot of action potentials from a representative cell. Note generation of SPW-R–associated spikes by local application of muscimol into stratum oriens. *Right* shows a ripple-associated antidromic action potential from that cell. (*C*) Increased sharp wave ripple-associated firing of eight pyramidal cells (three participators and five nonparticipators) in the presence of diazepam. Firing outside SPW-Rs was not changed. (*D*) Absolute change in SPW-R–associated firing before and after diazepam in WT (*Left*) and $GABA_AR$ $\alpha2^{H101R}$ (*Right*). Note the absence of diazepam effect in cells with benzodiazepine-insensitive α2-subunits.

selection of pyramidal cells during fast network oscillations (8, 33, 34). However, this model is unable to explain the existence of antidromic action potentials. Two alternative models have suggested that ectopic spikes originating in either the axon (35) or the basal dendrites (36) are crucial for the organization of ripple oscillations. We, therefore, used a modeling approach to tackle these questions. A network model of the CA1 region should explain these features in a self-consistent manner.

i) The field potential oscillates at more than ~150 Hz, waxing and waning in amplitude.
ii) Somatic pyramidal cell action potentials are rare during SPW-Rs (Figs. 1 and 2).
iii) Participating spikes are, on average, phase-locked to the local SPW-R field potential (Fig. 1 *C* and *E*).
iv) Participating spikes arise from an initial hyperpolarization and show characteristics of antidromic spikes (Fig. 3).
v) Participating spikes are more apt to occur in pyramidal cells in which perisomatic synaptic inhibition has been reduced (Fig. 5 *C* and *D*).
vi) Ripple frequency EPSPs occur in both interneurons (Fig. 4 *E* and *F*) and pyramidal cells (37), indicating that the pyramidal cell axonal plexus is indeed generating a high-frequency output.
vii) Spikelets occur very rarely in pyramidal cells during SPW-Rs, which contrasts previous network simulations (35).

How do we reconcile these observations (particularly *vii*)? One solution is to suppose that the fast oscillation is, indeed, generated in the axonal plexus but that spike generation and coupling occur in fine axonal branches (21, 38). We postulate that these branches are connected to main axonal trunks with a low safety factor (21, 39), and therefore, only a small fraction of the plexus spikes have a chance of producing antidromic action potentials (*SI Materials and Methods* and Fig. S9*A*). If gap junctions were, instead, all located on the main axon, then a mixture of full spikes and large (often >5 mV) spikelets would occur at the soma (contrary to experiment). The sequence of events in the model (Fig. 8) can be visualized in this way: when axonal gap junctions are open, the fine axonal plexus generates a high-frequency network oscillation that does not (by itself) require chemical synapses (35, 40). The orthodromic output of the axonal plexus induces rhythmic high-frequency EPSPs in both pyramidal cells and interneurons, and interneurons follow this input at high frequency (27) (Fig. S9*B*). The net synaptic input to pyramidal cells will then be alternating compound EPSPs and inhibitory postsynaptic potentials (IPSPs) (Fig. 8). In addition, some of the fine-plexus spikes are able to invade the main axon and lead to antidromic spikes—the participating spikes. The hyperpolarization before a participating spike is also supported by a burst of spikes in axoaxonic interneurons (similar to what is observed in vivo) (11). In the model, blocking synaptic inhibition in a particular pyramidal cell can (in at least some cells) convert a nonparticipating cell into a participating cell (Fig. S6). Although inhibition indeed plays a role in controlling antidromic discharges of pyramidal cells during SPW-Rs (as also observed during experiments) (Fig. 5 *C* and *D*), the dominant effect in the model is failure of spike propagation (e.g., branch-point failures). We were not able to configure any inhibitory circuitry that would by itself allow sparse SPW-R–associated firing while not resulting in large spikelets at the same time.

Thus, the model not only reproduces our experimental findings but provides a coherent understanding of the network interactions involved in assembly formation during SPW-Rs.

Discussion

We show that CA1 pyramidal cells fall into two functionally distinct classes with respect to the formation of transient oscillating cell assemblies. All recorded pyramidal cells had similar intrinsic properties and received strong somato-dendritic inhibition during SPW-R events. Participating cells, however, expressed antidromic action potentials with precise coupling to ripple oscillations. Interestingly, the occurrence of putative ectopic spikes in vivo has recently been reported for CA1 pyramidal cells (14). Ectopic spikes and inhibitory potentials have also been described during SPW-Rs in vitro (15). Our present work suggests an unexpected mechanism of pyramidal cell recruitment during fast network oscillations. In our proposed model, somatic spikes during SPW-Rs originate in distal axonal compartments of selected pyramidal cells forming an axonally connected cluster. After invading the main axonal trunk, action potentials will propagate into both directions, exciting downstream target neurons and causing antidromic somatic spikes that might invade the dendrite and facilitate synaptic plasticity. Another surprising finding is the dual role of $GABA_A$ receptors, which suppress background activity and promote axonal spike generation in participating neurons.

Ripple-Associated Spikes in Pyramidal Cells Are Antidromic Spikes. Cells participating in high-frequency oscillations are distinguished by ectopically generated action potentials that are entrained with millisecond precision. Ripple-associated action potentials are generated in the axon and invade the somatic recording site antidromically, which was shown by their typical waveform, IS-SD interval, notches, and resistance to hyperpo-

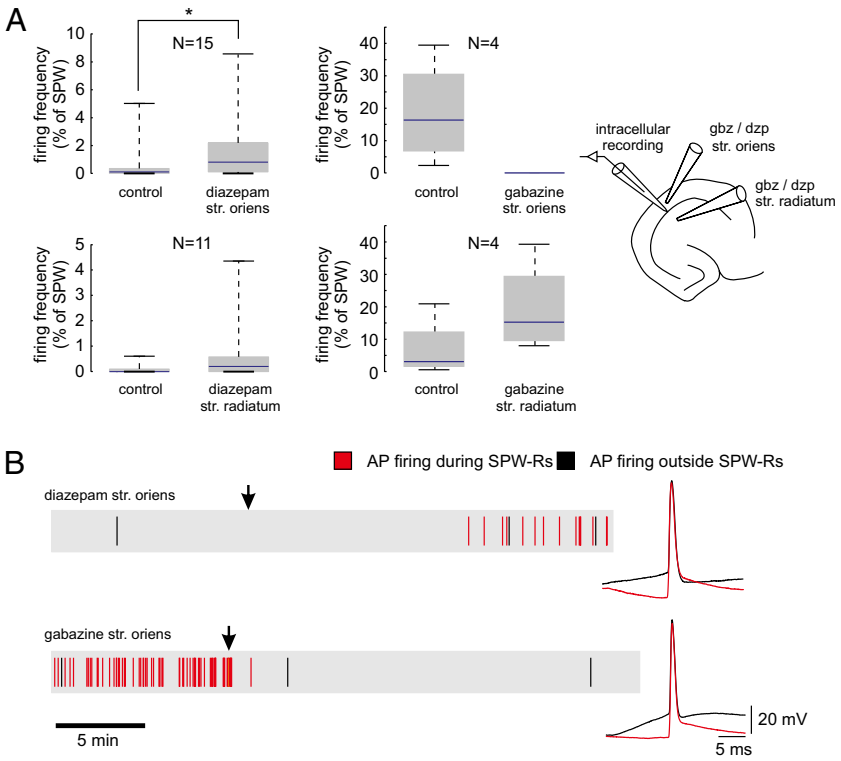

Fig. 7. Participation of pyramidal cells during SPW-Rs depends on a layer-specific GABAergic input. (*A*) Experimental setup showing the intracellular recording pipette in the stratum pyramidale and two positions of application pipettes in stratum radiatum and stratum oriens, respectively (*Right*). (*Left*) Increased firing of eight participators and four of seven nonparticipating cells on application of diazepam into stratum oriens (*Upper*). There was no significant effect with application of diazepam into stratum radiatum (*Lower*; four participators and seven nonparticipating cells). (*Right*) SPW-R–associated firing ceases with gabazine application into stratum oriens (*Upper*). Firing persists with gabazine in stratum radiatum (*Lower*). (*B*) Raster plot of action potentials from representative cells. (*Upper*) Recruitment of a nonparticipating cell with diazepam in stratum oriens. (*Lower*) Participating cell application of gabazine into stratum oriens. *Right* shows typical coupled (red) and noncoupled (black) action potentials from the respective cells.

larization (16, 19–23). As an alternative mechanism, ectopic spikes have been suggested to originate in dendrites (41), and dendritic spikes have been reported during SPW-Rs in vivo (42). However, the vast majority of SPW-R–coupled action potentials in our in vitro model must be generated in the axon. Somatic spikes of dendritic origin have normal action potential waveform and threshold (43), are blocked by somatic hyperpolarization (43, 44), and should not be abolished by disinhibition with gabazine (42). In line with these results, we were unable to model the present observations using dendritically generated action potentials (*SI Materials and Methods*).

Dual Role of $GABA_A$ Receptors. The distinction between participating and nonparticipating cells depends on two different GABAergic mechanisms. First, all pyramidal cells receive equally strong perisomatic and dendritic GABAergic input during SPW-Rs, ensuring sparse firing and high signal to noise ratio. Second, release of GABA within active networks facilitates spike generation in remote axonal compartments (23, 45). Collective evidence for this notion comes from the positive modulation of spiking by muscimol and diazepam, the counterintuitive block of SPW-R–coupled spikes by application of gabazine into stratum oriens, and the absent effect of benzodiazepines in $\alpha 2^{H101R}$ mice (29, 30). We suggest that, during SPW-Rs, the spike-promoting release of GABA results from the intense activation of GABAergic interneurons in stratum oriens (11, 26).

Modeling Provides a Mechanistic Understanding of Pyramidal Cell Recruitment. To put our cellular observations into a network context, we used multicompartment modeling of the CA1 network. According to the model, the very fast rhythm is generated within the axonal plexus, predominantly in smaller branches (38). Some of these spikes succeed in invading the main axonal trunk and also propagate antidromically to the soma, where they can be recorded as participating action potentials. Most of the plexus spikes do not, however, invade the main axonal trunk (39). The output of CA1 axons is also recurrently fed back onto local interneurons as well as CA1 basal dendrites (37), resulting in high-frequency synaptic currents in these structures. In addition, somatic inhibitory potentials at ripple frequency (8, 9) narrow the time window during which successfully propagating ripple-associated spikes do occur (46). In the model, however, synaptic inhibition is not the sole factor that controls somatic firing; branch-point failures were even more important. Several other models have proposed that neuronal synchronization during fast oscillations can result from nonlinear dendritic integration (36) or excitatory–inhibitory feedback loops (33, 34). Although the present observations show a crucial role for excitatory–inhibitory interactions, they also provide clear evidence for antidromic spikes that are not captured by other models.

The proposed mechanism of spike generation has several implications for signal processing in the network. The occurrence of a participating spike in the soma indicates that the action potential has reached the main axonal trunk. Only then will it propagate to downstream structures (such as the subiculum) as well as back-propagate into the dendritic tree. A participating spike could, thereby, link plastic changes of excitatory synaptic inputs to a pyramidal cell with the main axonal outputs—although the antidromic spike is not caused by the synaptic inputs in question. This concept would be a variation on classical Hebbian synaptic plasticity, in which synaptic inputs cause the action

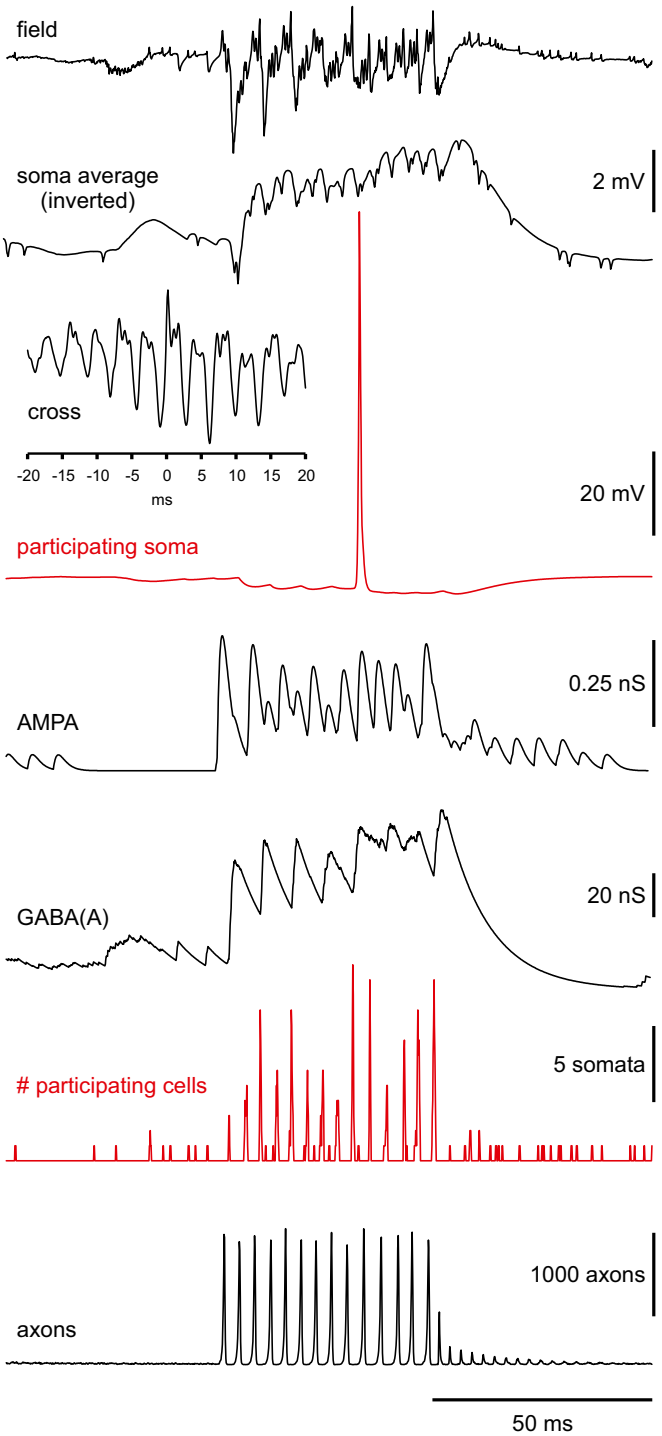

Fig. 8. A computer model of SPW-Rs reproduces cellular recruitment during ripples. Multicompartment modeling of the CA1 network was used to gain a mechanistic understanding of pyramidal cell recruitment during SPW-Rs. The model includes CA1 pyramidal cells and three interneuron subtypes connected by chemical and electrical synapses (*Materials and Methods* and *SI Materials and Methods*). Generation of ~200-Hz oscillations (lines 1 and 2) is based on gap junctions between pyramidal cell axons that fire at ripple frequency during network events (bottom trace). Although basket cells fire during most ripple cycles (~2 ms after pyramidal cell somata), only a minority of pyramidal cells participate in individual network events (line 6). Thus, only a few of the axonal spikes successfully invade the soma antidromically (line 3) (Fig. S9). Rhythmic synaptic conductances of pyramidal cells are dominated by inhibitory inputs that alternate with rhythmic excitatory inputs of much smaller amplitude (lines 4 and 5). In the model, perisomatic inhibition helps to control discharge probability and spike timing during SPW-Rs (Fig. S6). *Inset* shows cross-correlation of the participating cell signal with the field. Note that increased antidromic spike rates caused by tonic GABAergic currents in stratum oriens (as suggested by our experimental findings) are also fundamental for the organization of SPW-Rs in the model.

potentials that, then, can strengthen those inputs. Interestingly, activity-dependent plasticity of ectopic spike generation has recently been reported for hippocampal interneurons (21), indicating that axons might be more important for signal integration than previously thought.

In summary, we show that principal hippocampal neurons fall into two distinct classes with respect to local network activity. Members of oscillating assemblies show an unusual mechanism of ectopic action potential generation, whereas somatodendritic inhibition suppresses background activity in the network during SPW-R events. Our findings provide a mechanism of assembly formation in oscillating networks. They may be relevant for the study of SPW-R–associated memory consolidation in the hippocampus.

Materials and Methods

The study was conducted in compliance with German law and with the approval of the state governments of Baden-Württemberg and Berlin. Experiments were performed on adult male C57Bl6 mice (4–12 wk). In experiments using $\alpha 2^{H101R}$ mice (ref. 32 has additional information on the generation of this mouse line), animals of both sexes were used.

Slice Preparation. Brains of ether-anesthetized mice were removed and cooled to 1–4 °C in artificial cerebrospinal fluid (ACSF) containing 124 mM NaCl, 3 mM KCl, 1.8 mM $MgSO_4$, 1.6 mM $CaCl_2$, 10 mM glucose, 1.25 mM NaH_2PO_4, and 26 mM $NaHCO_3$ saturated with 95% O_2/5% CO_2 (pH 7.4 at 37 °C). After removal of the cerebellum and frontal brain structures, we cut horizontal slices of 450 μm on a vibratome (VT 1000 S; Leica). Slices were allowed to recover for at least 2 h in a Haas-type interface recording chamber at 35 ± 0.5 °C before starting the experiments. Most slices used for recordings were from the middle part of the hippocampus. These procedures slightly differed for slices that were used for recordings in a submerged chamber (*SI Materials and Methods*) (24).

Electrophysiology and Labeling. Extracellular recordings from CA1 pyramidal layer were performed with glass electrodes (tip diameter > 5 μm; filled with ACSF). Potentials were amplified 100 times with an EXT 10–2F amplifier (NPI Electronic), low pass-filtered at 3 kHz, and digitized at 5–10 kHz for offline analysis (1401 interface; CED). These parameters slightly differed for extracellular recordings in the submerged condition (*SI Materials and Methods*) (24).

Whole-cell recordings were performed using a Multiclamp 700B amplifier (Axon Instruments). Borosilicate glass electrodes (2–5 MΩ) were filled with 135 mM K-gluconate, 10 mM Hepes, 2 mM Mg-ATP, 20 mM KCl, and 0.2 mM EGTA, pH 7.2 (KOH). Cells were identified using infrared differential interference contrast video microscopy and characterized by de- and hyperpolarizing current steps (200–1,000 ms). We included only cells showing typical fast-spiking discharge characteristics of interneurons. Series resistance R_s was monitored continuously throughout experiments; cells were rejected if R_s was >20 MΩ or varied more than ±30% during recordings. Potentials indicated are liquid junction potential-corrected (calculated at ~14 mV). Intracellular (sharp electrode) and juxtacellular recordings were performed in the vicinity of the extracellular electrode with a SEC-05 LX amplifier (NPI Electronic) in bridge mode. Potentials were amplified 10 times, low pass-filtered at 8 kHz, and sampled at 20 kHz. Sharp electrodes for intracellular recordings (OD at 1.5 mm) were filled with either 2 M KAc (pH 7.35; n = 153) or 1 M KCl (n = 14) and had a resistance of 60–110 MΩ. After impalement, we injected negative current until the cell stabilized and then, gradually reduced the current injection to zero. Bridge balance was repeatedly adjusted by optimizing the voltage response to small (–200 pA) square current pulses. Offset potentials were determined and subtracted at the end of the experiment. Intrinsic properties were assessed by negative and positive current pulses of 400 ms duration. Cells were accepted if they had a resting membrane potential more negative than –55 mV, over-

shooting action potentials, input resistance >20 MΩ, and a stable current-free recording of at least 30 min.

Electrical stimulation was performed with bipolar platinum/iridium wire electrodes that were located in the alveus or the Schaffer collaterals, respectively. Monopolar square pulses of 100 μs duration were delivered at a strength calibrated to evoke reliable action potential firing.

Juxtacellular recordings were performed with glass electrodes (15–25 MΩ) filled with 3% (wt/vol) Biocytin (Sigma) in 0.5 M NaCl. After unit recording, individual cells were filled using the juxtacellular labeling method (47).

Drugs and Chemicals. Drugs were purchased from Sigma and RBI/Tocris, and the fluorescent dye fluorescein was purchased from Invitrogen. Pharmacological agents (stock solutions dissolved in ACSF) were either added to the bath solution (20 μM diazepam) or were applied locally by leakage from large extracellular glass electrodes (tip diameter ~ 15 μm). Local application electrodes were placed on the surface of the slice in stratum radiatum, stratum oriens, or the alveus of CA1 (20 μM diazepam, 10 μM gabazine, 5 μM muscimol, 100 μM 4-AP). In one experiment, picrotoxin (200 μM) was added to the intracellular solution for the selective manipulation of impaled cells.

Histological Procedures. Neurobiotin- or biocytin-filled cells were visualized using standard procedures (fluorescence and 3–3′ diaminobenzidine tetrahydrochloride staining). Detailed methods regarding tissue processing are in *SI Materials and Methods*. Samples were analyzed using an Olympus BX61 microscope (Olympus). One cell (Fig. 4*A*) was reconstructed with the aid of Neurolucida software (Microbrightfield) using a 100× oil objective. Subsequent EM was carried out on four cells as described in detail elsewhere (48). Serial sections were cut with an ultramicrotome (EM UC6; Leica) and analyzed for synaptic contacts of biocytin-labeled axon terminals using a Philips CM 100 electron microscope.

Data Processing and Analysis. Data were sampled with the Spike2 and Signal program (CED) and analyzed offline using custom written routines in Matlab (MathWorks). A detailed description is in *SI Materials and Methods*.

Statistics. Quantitative results are given as mean ± SEM or as median and the first and third quartiles (P_{25} and P_{75}). Parametric tests were used if groups passed a normality test, and otherwise, nonparametric statistics were used. A P value < 0.05 was regarded as significant.

Simulation Methods. We constructed a CA1 network model to explore possible physiological mechanisms for the generation of SPW-Rs and associated participating somatic action potentials. At this preliminary stage, we were interested only in basic cellular, synaptic, and gap junctional contributions to general features of the events, such as ripple shape, action potential timing, and site of origin of the participating action potentials; we did not attempt to make quantitative predictions concerning the precise values of synaptic and intrinsic membrane conductances or anatomical features. The style of modeling is as in the works by Traub et al. (49) and Roopun et al. (50) (a detailed description of the model is in *SI Materials and Methods*). The network model contains CA1 pyramidal neurons with branching axons (4,000), fast-spiking basket cells (200), bistratified (dendrite-contacting, fast-spiking) interneurons (100), and axoaxonic cells (40); oriens-lacunosum moleculare interneurons were omitted, because in vivo data suggest their silence during SPW-Rs (11), and other interneurons were omitted for the sake of simplicity. Preliminary simulations were performed, varying the synaptic and gap junctional conductances, synaptic connectivity, axonal branching patterns, and sites of axonal gap junctions.

The field potential was approximated using two methods. First, field potentials were computed using a weighted average of pyramidal cell transmembrane currents [details in the work by Traub et al. (49)]. Second, average values of pyramidal cell somatic voltages were inverted.

The simulation program, CA1netax.f, was written in Fortran with mpi instructions for operating in a parallel environment and run on 20 processors of an AIX cluster at the IBM T. J. Watson Research Center. A fixed integration time step of 2 μs was used. Simulation of 250 ms of activity required about 1.25 h of central processing unit time. Copies of the code are available on request from R.D.T. (rtraub@us.ibm.com).

Quantities Saved by the Simulation Program for Plotting and Analysis. The program saves a number of signals, including average values of pyramidal cell somatic voltages (inverted to resemble a field potential), somatic, axonal, and dendritic potentials in selected pyramidal cells and interneurons, average somatic potentials of interneuron populations, and the number of overshooting pyramidal cell distal axons and somata.

ACKNOWLEDGMENTS. We thank Drs. N. Spruston, H. Möhler, U. Heinemann, and C. Bruehl for fruitful discussions and Barbara Joch, Marlies Kaiser, Alexander Lehmann, Anne Rossmann, and Dr. Susanne Reichinnek for excellent technical assistance. This work was supported by Bundesministerium für Bildung und Forschung (BMBF) (Bernstein Centre for Computational Neuroscience Heidelberg-Mannheim) and Deutsche Forschungsgemeinschaft (SFB 636). E.K.W. is a fellow of the MD/PhD Program at the University of Heidelberg. D.S. is supported by BMBF (Bernstein Centre for Computational Neuroscience Berlin) and Deutsche Forschungsgemeinschaft Grants SFB 618, 665, and EXC 257. M.F. is supported by the Hertie Foundation. R.D.T. was supported by National Institutes of Health/National Institute of Neurological Disorders and Stroke Grants NS44138 and N5062955, IBM Corp., and the Alexander von Humboldt Stiftung.

1. Hebb D (1949) *The Organization of Behavior* (Wiley, New York).
2. Grillner S (2006) Biological pattern generation: The cellular and computational logic of networks in motion. *Neuron* 52:751–766.
3. Womelsdorf T, et al. (2007) Modulation of neuronal interactions through neuronal synchronization. *Science* 316:1609–1612.
4. Harris KD, Csicsvari J, Hirase H, Dragoi G, Buzsáki G (2003) Organization of cell assemblies in the hippocampus. *Nature* 424:552–556.
5. Buzsáki G, Draguhn A (2004) Neuronal oscillations in cortical networks. *Science* 304: 1926–1929.
6. Barnes CA, Suster MS, Shen J, McNaughton BL (1997) Multistability of cognitive maps in the hippocampus of old rats. *Nature* 388:272–275.
7. Wilson MA, McNaughton BL (1994) Reactivation of hippocampal ensemble memories during sleep. *Science* 265:676–679.
8. Ylinen A, et al. (1995) Sharp wave-associated high-frequency oscillation (200 Hz) in the intact hippocampus: Network and intracellular mechanisms. *J Neurosci* 15:30–46.
9. Csicsvari J, Hirase H, Czurkó A, Mamiya A, Buzsáki G (1999) Oscillatory coupling of hippocampal pyramidal cells and interneurons in the behaving rat. *J Neurosci* 19: 274–287.
10. Maier N, Nimmrich V, Draguhn A (2003) Cellular and network mechanisms underlying spontaneous sharp wave-ripple complexes in mouse hippocampal slices. *J Physiol* 550: 873–887.
11. Klausberger T, et al. (2003) Brain-state- and cell-type-specific firing of hippocampal interneurons in vivo. *Nature* 421:844–848.
12. Ellender TJ, Nissen W, Colgin LL, Mann EO, Paulsen O (2010) Priming of hippocampal population bursts by individual perisomatic-targeting interneurons. *J Neurosci* 30: 5979–5991.
13. Draguhn A, Traub RD, Schmitz D, Jefferys JG (1998) Electrical coupling underlies high-frequency oscillations in the hippocampus in vitro. *Nature* 394:189–192.
14. Epsztein J, Lee AK, Chorev E, Brecht M (2010) Impact of spikelets on hippocampal CA1 pyramidal cell activity during spatial exploration. *Science* 327:474–477.
15. Papatheodoropoulos C (2008) A possible role of ectopic action potentials in the in vitro hippocampal sharp wave-ripple complexes. *Neuroscience* 157:495–501.
16. Schmitz D, et al. (2001) Axo-axonal coupling. a novel mechanism for ultrafast neuronal communication. *Neuron* 31:831–840.
17. Fricker D, Miles R (2000) EPSP amplification and the precision of spike timing in hippocampal neurons. *Neuron* 28:559–569.
18. Storm JF (1987) Action potential repolarization and a fast after-hyperpolarization in rat hippocampal pyramidal cells. *J Physiol* 385:733–759.
19. Hu W, et al. (2009) Distinct contributions of Na(v)1.6 and Na(v)1.2 in action potential initiation and backpropagation. *Nat Neurosci* 12:996–1002.
20. Coombs JS, Curtis DR, Eccles JC (1957) The interpretation of spike potentials of motoneurones. *J Physiol* 139:198–231.
21. Sheffield ME, Best TK, Mensh BD, Kath WL, Spruston N (2011) Slow integration leads to persistent action potential firing in distal axons of coupled interneurons. *Nat Neurosci* 14:200–207.
22. Colbert CM, Johnston D (1996) Axonal action-potential initiation and Na+ channel densities in the soma and axon initial segment of subicular pyramidal neurons. *J Neurosci* 16:6676–6686.
23. Avoli M, Methot M, Kawasaki H (1998) GABA-dependent generation of ectopic action potentials in the rat hippocampus. *Eur J Neurosci* 10:2714–2722.
24. Maier N, Morris G, Johenning FW, Schmitz D (2009) An approach for reliably investigating hippocampal sharp wave-ripples in vitro. *PLoS One* 4:e6925.
25. Whittington MA, Traub RD, Faulkner HJ, Stanford IM, Jefferys JG (1997) Recurrent excitatory postsynaptic potentials induced by synchronized fast cortical oscillations. *Proc Natl Acad Sci USA* 94:12198–12203.
26. Glykys J, Mody I (2007) The main source of ambient GABA responsible for tonic inhibition in the mouse hippocampus. *J Physiol* 582:1163–1178.
27. Traub RD, et al. (2003) GABA-enhanced collective behavior in neuronal axons underlies persistent gamma-frequency oscillations. *Proc Natl Acad Sci USA* 100: 11047–11052.

28. Romo-Parra H, Treviño M, Heinemann U, Gutiérrez R (2008) GABA actions in hippocampal area CA3 during postnatal development: Differential shift from depolarizing to hyperpolarizing in somatic and dendritic compartments. *J Neurophysiol* 99:1523–1534.
29. Ruiz A, et al. (2003) GABAA receptors at hippocampal mossy fibers. *Neuron* 39: 961–973.
30. Trigo FF, Marty A, Stell BM (2008) Axonal GABAA receptors. *Eur J Neurosci* 28: 841–848.
31. Nusser Z, Sieghart W, Benke D, Fritschy JM, Somogyi P (1996) Differential synaptic localization of two major gamma-aminobutyric acid type A receptor alpha subunits on hippocampal pyramidal cells. *Proc Natl Acad Sci USA* 93:11939–11944.
32. Löw K, et al. (2000) Molecular and neuronal substrate for the selective attenuation of anxiety. *Science* 290:131–134.
33. Buzsáki G, Chrobak JJ (1995) Temporal structure in spatially organized neuronal ensembles: A role for interneuronal networks. *Curr Opin Neurobiol* 5:504–510.
34. Geisler C, Brunel N, Wang XJ (2005) Contributions of intrinsic membrane dynamics to fast network oscillations with irregular neuronal discharges. *J Neurophysiol* 94: 4344–4361.
35. Traub RD, Bibbig A (2000) A model of high-frequency ripples in the hippocampus based on synaptic coupling plus axon-axon gap junctions between pyramidal neurons. *J Neurosci* 20:2086–2093.
36. Memmesheimer RM (2010) Quantitative prediction of intermittent high-frequency oscillations in neural networks with supralinear dendritic interactions. *Proc Natl Acad Sci USA* 107:11092–11097.
37. Tejero-Cantero A, et al. (2009) Synaptic contributions to in vitro hippocampal sharp-wave ripples. *BMC Neurosci* 10(Suppl 1):278.
38. Knowles WD, Schwartzkroin PA (1981) Axonal ramifications of hippocampal Ca1 pyramidal cells. *J Neurosci* 1:1236–1241.
39. Goldstein SS, Rall W (1974) Changes of action potential shape and velocity for changing core conductor geometry. *Biophys J* 14:731–757.
40. Nimmrich V, Maier N, Schmitz D, Draguhn A (2005) Induced sharp wave-ripple complexes in the absence of synaptic inhibition in mouse hippocampal slices. *J Physiol* 563:663–670.
41. Spencer WA, Kandel ER (1961) Electrophysiology of hippocampal neurons. IV. Fast prepotentials. *J Neurophysiol* 24:272–285.
42. Kamondi A, Acsády L, Buzsáki G (1998) Dendritic spikes are enhanced by cooperative network activity in the intact hippocampus. *J Neurosci* 18:3919–3928.
43. Gasparini S, Migliore M, Magee JC (2004) On the initiation and propagation of dendritic spikes in CA1 pyramidal neurons. *J Neurosci* 24:11046–11056.
44. Golding NL, Spruston N (1998) Dendritic sodium spikes are variable triggers of axonal action potentials in hippocampal CA1 pyramidal neurons. *Neuron* 21:1189–1200.
45. Keros S, Hablitz JJ (2005) Ectopic action potential generation in cortical interneurons during synchronized GABA responses. *Neuroscience* 131:833–842.
46. Dodla R, Rinzel J (2006) Enhanced neuronal response induced by fast inhibition. *Phys Rev E Stat Nonlin Soft Matter Phys* 73:010903.
47. Pinault D (1996) A novel single-cell staining procedure performed in vivo under electrophysiological control: Morpho-functional features of juxtacellularly labeled thalamic cells and other central neurons with biocytin or Neurobiotin. *J Neurosci Methods* 65:113–136.
48. Markram H, Lübke J, Frotscher M, Roth A, Sakmann B (1997) Physiology and anatomy of synaptic connections between thick tufted pyramidal neurones in the developing rat neocortex. *J Physiol* 500:409–440.
49. Traub RD, et al. (2005) Single-column thalamocortical network model exhibiting gamma oscillations, sleep spindles, and epileptogenic bursts. *J Neurophysiol* 93: 2194–2232.
50. Roopun AK, et al. (2010) A nonsynaptic mechanism underlying interictal discharges in human epileptic neocortex. *Proc Natl Acad Sci USA* 107:338–343.